Chinese Chemical Letters 34 (2023) 107643

Contents lists available at ScienceDirect

Chinese Chemical Letters

journal homepage: www.elsevier.com/locate/cclet

Enhancing hydrogen evolution reaction performance of transition metal doped two-dimensional electride Ca_2N

Baoyu Liu[a], Ziqiang Chen[a], Rui Xiong[a], Xuhui Yang[b], Yinggan Zhang[c], Teng Xie[a], Cuilian Wen[a,*], Baisheng Sa[a,*]

[a] Multiscale Computational Materials Facility, and Key Laboratory of Eco-materials Advanced Technology, College of Materials Science and Engineering, Fuzhou University, Fuzhou 350100, China
[b] College of Environmental Science and Engineering, Fujian Key Laboratory of Pollution Control & Resource Reuse, Fujian Normal University, Fuzhou 350007, China
[c] College of Materials, Fujian Provincial Key Laboratory of Theoretical and Computational Chemistry, Xiamen University, Xiamen 361005, China

ARTICLE INFO

Article history:
Received 22 May 2022
Revised 11 June 2022
Accepted 23 June 2022
Available online 1 July 2022

Keywords:
Two-dimensional electride
Ca_2N
Density functional theory calculations
Hydrogen evolution reaction
Transition metal doping

ABSTRACT

Two-dimensional electride Ca_2N has strong electron transfer ability and low work function, which is a potential candidate for hydrogen evolution reaction (HER) catalyst. In this work, based on density functional theory calculations, we adopt two strategies to improve the HER catalytic activity of Ca_2N monolayer: introducing Ca or N vacancy and doping transition metal atoms (TM, refers to Ti, V, Cr, Mn, Fe, Zr, Nb, Mo, Ru, Hf, Ta and W). Interestingly, the Gibbs free energy ΔG_{H*} of Ca_2N monolayer after introducing N vacancy is reduced to -0.146 eV, showing good HER catalytic activity. It is highlighted that, the HER catalytic activity of Ca_2N monolayer can be further enhanced with TM doping, the Gibbs free energy ΔG_{H*} of single Mo and double Mn doped Ca_2N are predicted to be 0.119 and 0.139 eV, respectively. The present results will provide good theoretical guidance for the HER catalysis applications of two-dimensional electride Ca_2N monolayer.

With the continuous progress of global industrialization, more and more energy is consumed, which makes the global energy crisis more serious and brings great pressure to the ecological environment [1–4]. There is an urgent need for efficient and ecofriendly energy conversion technology to achieve the sustainability of human society. Hydrogen, as a typical carrier of clean and renewable energy [5,6], has been regarded as an important substitute for fossil fuels and can solve the increasingly serious ecological environment problems [7–9]. Electrocatalytic reduction of water by hydrogen evolution reaction (HER) is an effective method in various potential hydrogen reduction technologies [10–12], and the key factor in this process is efficient electrocatalysts. At present, the most widely used electrocatalyst is noble metal Pt [13–16]. However, the high cost and scarcity of Pt seriously hinders its large-scale industrial application [11,17-19]. Therefore, it is extremely important to find a rich and economical electrocatalyst on the earth to replace the Pt metal. In the past years, many novel two-dimensional (2D) materials have been proposed as effectively HER catalysts, such as, transition metal dichalcogenides (TMDCs) [8,10,11], transition metal nitrides or carbides (MXenes) [20,21], transition metal borides (MBenes) [7,22], graphene-like carbon nitrides (g-C_3N_4) [23], layered double hydroxides (LDHs) [24], monoatomic catalysts (SACs) [25,26] and two-dimensional electrides (2D-electrides) [27,28].

In recent years, inorganic electrides, an emerging kind of materials has been reported [29,30], which will bring great significance to the development of artificial materials. Electrides are a class of novel ionic compounds, which contain excess electrons distributed in crystal cavities playing the role of anions [31]. In electrides, the trapped electrons are usually loosely bounded and form unique electronic structure features, which make them present many excellent physical and chemical properties, such as high electron mobility, extremely low work function, strong electron-donating ability, and good oxidation activity and catalytic activity [29,30]. Due to these excellent properties, electrides have broad and promising application prospects, such as catalyst promoters or catalysts [32], battery electrode materials [33], electronic devices, superconductors [34] and new magnetic materials [35]. Especially in the field of catalysis, electrides contain excess electrons, which are easily to transfering to other substances, and attracting considerable attention toward various important chemical reactions.

* Corresponding authors.
E-mail addresses: clwen@fzu.edu.cn (C. Wen), bssa@fzu.edu.cn (B. Sa).

https://doi.org/10.1016/j.cclet.2022.06.066
1001-8417/

For example, the electride $[Ca_{24}Al_{28}O_{64}]^{4+}\cdot 4e^-$ (usually abbreviated as C12A7:e^-) shows the characteristics of low work function and strong electron transfer ability [36]. Ru-loaded C12A7:e^- (Ru/C12A7:e^-) is considered to be an efficient ammonia synthesis catalyst at low temperature and pressure, which can reduce the activation energy of ammonia synthesis reaction and enhance the dissociation of N_2 [37,38]. The electride Y_5Si_3 [39] also shows strong chemical activity, and Ru-loaded Y_5Si_3 (Ru/Y_5Si_3) is a highly efficient ammonia synthesis catalyst [40]. Rare-earth-based intermetallic electrides are proposed to be efficient ammonia synthesis catalysts as well, *e.g.*, LaRuSi [41] and Ru-loaded LaNiSi [42]. Moreover, Cu-based intermetallic electride $LaCu_{0.67}Si_{1.33}$ [43] exhibits strong electron transfer ability and low work function, which can reduce the activation energy of chemical reaction and promote the dissociation of hydrogen molecules and shows good catalytic activity in various hydrogenation reactions. These reported electrides have several common characteristics, such as strong electron transfer ability, low work function, chemical stability and good chemical reaction activity, which are beneficial for the catalysis performance. However, due to the limited environment stabilities [27,42], the discovery and development of electrides for high performance catalysis is still on going.

Recently, a layered electride material, dicalcium nitride, with 2D anionic electrons has been reported [31]. This layered electride has a chemical formula of Ca_2N, which can be rewritten as $[Ca_2N]^+\cdot e^-$ to reflect the anionic electron delocalized in the interstitial space between two Ca_2N layers. Since Ca_2N has a low work function of 2.6 eV and a high electron mobility of 520 $cm^2\ V^{-1}\ s^{-1}$ [44,45], it would be effective in transferring electrons into electrochemical reaction. It is noted that obtaining Ca_2N monolayers *via* bulk exfoliation can be achieved based on the previous research about the cleavage energy and strength [46,47]. Furthermore, it is motivated by a self-passivated 2D monolayer di-hafnium sulfide electride ($[Hf_2S]^{2+}\cdot 2e^-$) [27], which demonstrating good HER performance with excellent long-term sustainability and no degradation in performance [27]. Therefore, the exploration and investigation of monolayer Ca_2N as anticapted high performance HER catalyst is of great interest and importance.

In this work, based on density functional theory calculations using the Vienna *ab initio* simulation package (VASP) [48] and dealt with the ALKEMIE platform [49,50], we explored the HER catalytic performance of 2D electride Ca_2N monolayer. The calculation details of Supporting information can be referred to for specific calculation methods. We proposed two effective methods to improve the HER catalytic activity of Ca_2N monolayer: vacancy defect engineering and transition metal doping. It finds that both way can improve the HER catalytic activity of Ca_2N monolayer to a favorable level with the Gibbs free energy $|\Delta G_{H*}| < 0.2$ eV.

The 2D crystal structure of Ca_2N monolayer with the space group of $P\bar{3}m1$ consists of one N layer sandwiched between two Ca layers, as shown in Fig. 1a. Each surface Ca atom is coordinated to three N atoms, while each N is covalently bonded to six Ca atoms. The optimized lattice parameter of the Ca_2N monolayer is $a = b = 3.607$ Å, and the optimized Ca-N bong length is 2.433 Å. The results agree well with previously literatures [31,51]. The stability of the 2D structure framework is a prerequisite for long-term operation. Therefore, we have to estimate the stability of the Ca_2N monolayer.

First of all, the dynamic, thermodynamic, and geometric stability of Ca_2N monolayer have been confirmed by performing accurate phonon calculations and AIMD simulations in the previous reported literatures [31,45,47,52]. Moreover, we also carried out AIMD simulations to verify the dynamic and geometric stability of Ca_2N monolayer, as shown in Fig. S1 (Supporting information). The results are consistent with the previous reported literatures as well, suggesting good thermodynamic stability of Ca_2N monolayer. An understanding on the electron transfer efficiency of Ca_2N monolayer in the electrocatalytic reactions can be gained by analyzing the density of states (DOS). Fig. S2 (Supporting information) shows the total DOS and PDOS of Ca_2N monolayer. Obviously, Ca_2N monolayer exhibits metallic conductivity with the Fermi energy falling into continuum energy states, which is consistent with previous works [46,47]. According to PDOS, the metallic electronic structure nature of Ca_2N monolayer is mainly contributed by the Ca-d and N-p orbitals around the Fermi level.

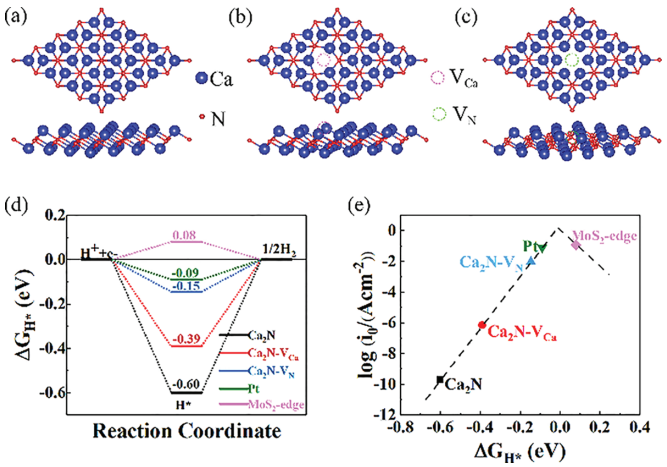

Fig. 1. Top and side views of (a) pristine Ca_2N, (b) Ca_2N-V_{Ca} and (c) Ca_2N-V_N. (d) Calculated Gibbs free energy diagram of HER for pristine Ca_2N, Ca_2N-V_{Ca} and Ca_2N-V_N with the hydrogen coverage of 1/16. (e) Volcano curve of exchange current density i_0 as a function of ΔG_{H*} for intrinsic and defective Ca_2N.

To explore the catalytic activity for HER performance, we first examined the adsorption behavior of H atoms on the surface of Ca_2N monolayer to locate the most favorable adsorption sites. The optimized active site for H adsorption is on top of the middle of three Ca atoms on the surface, as show in Fig. S3a (Supporting information). The Gibbs free energy for hydrogen adsorption (ΔG_{H*}) on Ca_2N monolayer is calculated to be −0.599 eV, which is far away from than the ideal value. Herein, an optimal HER activity can be achieved for an excellent catalyst when the absolute value of ΔG_{H*} ($|\Delta G_{H*}|$) is close to zero, indicating that the Gibbs free energy of adsorbed H is close to that of the reactant or product [7,8,10,11]. More negative ΔG_{H*} will result in a too strong bonding of adsorbed H to extract from the catalyst surface, while more positive ΔG_{H*} will make the protons bond to the surface of catalyst too weak and difficult. Therefore, both negative and positive ΔG_{H*} lead to slow HER kinetics. Generally, the criteria for judging whether a material possesses HER activity follows the classical rule of $|\Delta G_{H*}| < 0.2$ eV. Therefore, such relatively strong binding of atomic hydrogen indicates that the Ca_2N monolayer exhibits inertial HER activity.

We firstly introduced vacancy defects to improve the HER catalytic activity of Ca_2N monolayer. To avoid the influence of the periodical boundary conditions and improve computational accuracy, we built a $4 \times 4 \times 1$ supercell for the following study. In view of the structural characteristics and element composition of Ca_2N monolayer, we have considered two types of vacancies: Ca-vacancy in Ca_2N monolayer (short for Ca_2N-V_{Ca}) and N-vacancy in Ca_2N monolayer (short for Ca_2N-V_N), as shown in Figs. 1b and c, respectively. The calculated vacancy formation energy E_f according to Eqs. S1 and S2 (Supporting information) of Ca_2N-V_{Ca} and Ca_2N-V_N are 0.724 eV and 2.553 eV, respectively. Generally, the smaller positive value of the vacancy formation energy indicates the higher possibility for the formation of the vacancy. Therefore, it is evidently that Ca_2N-V_{Ca} shows greater possibility to form in Ca_2N monolayer

with a relatively low vacancy formation energy. Besides, we also carry out AIMD simulations to verify the dynamic and geometric stability of Ca_2N monolayer with Ca-vacancy and N-vacancy, as shown in Figs. S1b and c, respectively. The well maintained structures and narrow range fluctuating total energies suggest good thermodynamic stabilities of both Ca_2N-V_{Ca} and Ca_2N-V_N. As can be seen from the PDOS in Figs. S2b and c, Ca_2N-V_{Ca} and Ca_2N-V_N still present metallic properties and show good electronic conductivities.

For Ca_2N-V_{Ca}, the optimal active site for the adsorption of hydrogen atom is in the center of three Ca atoms and above the N atom around the Ca vacancy, as shown in Fig. S3b (Supporting information). On the other hand, for Ca_2N-V_N, the best active site for the adsorption of hydrogen atom is above the N vacancy, as shown in Fig. S3c (Supporting information). The Gibbs free energies for hydrogen adsorption for Ca_2N monolayer without and with vacancy are summarized in Fig. 1d, where the corresponding values for Pt (111) and MoS_2 edge are shown for reference as well [2,21,53]. The calculated ΔG_{H*} for Ca_2N-V_{Ca} and Ca_2N-V_N are -0.390 and -0.146 eV, respectively. The results indicate that the vacancies can promote the HER catalytic activity of Ca_2N monolayer. In particular, ΔG_{H*} of Ca_2N-V_N is calculated to be -0.146 eV, where the absolute value is smaller than 0.2 eV, indicating the potential high HER catalytic activity. The main reason for this phenomenon is that the presence of N vacancies reduces the number of anions, and more charges will accumulate around the Ca atoms around the N vacancies. The extra electrons of Ca_2N are beneficial for the HER process, which reduce the energy barrier of the catalytic reaction and make the catalytic reaction easier. Therefore, the introduction of vacancy defects can improve the HER catalytic activity of Ca_2N monolayer. Furthermore, Fig. 1e shows the volcano curve of exchange current density i_0 as a function of ΔG_{H*} refer to Nørskov's model [54], where the volcano peak corresponds to the best HER activity [55]. Obviously, the pristine Ca_2N is located around the left legs of the volcano curve, while the Ca_2N-V_N is near the peak of the volcano curve. However, compared with the common noble metal Pt catalyst (ΔG_{H*} = -0.090 eV) [2,53,56] and the non-noble metal compound MoS_2-edge (ΔG_{H*} = 0.080 eV) [2,56-58], the HER catalytic activity of Ca_2N-V_N is still a little bit lower. The Pt and MoS_2-edge activities are closer to the peak position of the volcano curve, which are consistent with the previously analysis [2,56]. It can be concluded that introducing vacancy defects can improve the catalytic activity of Ca_2N monolayer, however, it has not exceeded the catalytic activity of Pt and MoS_2-edge, which requires further improvements.

To further improve the catalytic activity of Ca_2N monolayer, we tried to change the HER chemical environment on the surface of Ca_2N monolayer by transition metal (TM) doping. As shown in Figs. 2a and b, we replaced a Ca atom with a TM atom in a $4 \times 4 \times 1$ Ca_2N supercell. Herein, 12 different TMs of Ti, Zr, Hf, V, Nb, Ta, Cr, Mo, W, Mn, Fe and Ru have been considered. As shown in Fig. 2c and Table S1 (Supporting information), among the 12 TM doped Ca_2N monolayers (1TM@Ca_2N), Ru doping Ca_2N monolayer shows the most positive formation energy E_f of 2.783 eV, and Hf doping presents the most negative E_f of -0.496 eV. It is worth noting that Ti and Zr doping show negative E_f of -0.454 eV and -0.389 eV, respectively, indicating that the Hf, Ti and Zr doping processes are exothermic and spontaneous. On the other hand, the formation energy of the other 9 TMs are greater than 0, indicating that the formation is endothermic. Nonetheless, except for Ru and Mn, the formation energies of other TMs have small positive values not greater than 2 eV, which indicates that the doping processes are still possible. In order to investigate the electronic properties of 1TM@Ca_2N, we display the total DOS and projected DOS plots for the 1TM@Ca_2N as depicted in Fig. S4 (Supporting information). It has been found that all these 12 kinds of 1TM@Ca_2N exhibit metallic conductivity with the Fermi energy falling into a continuum energy states. Fig. S5a (Supporting information) illustrates the charge transfer from TM to neighboring N atoms, which indicates that the substitution of doped TM makes some change in its structure. It is seen that TM-doping gives rise to the redistribution of the electron charge, which could play as the role of catalysis active center.

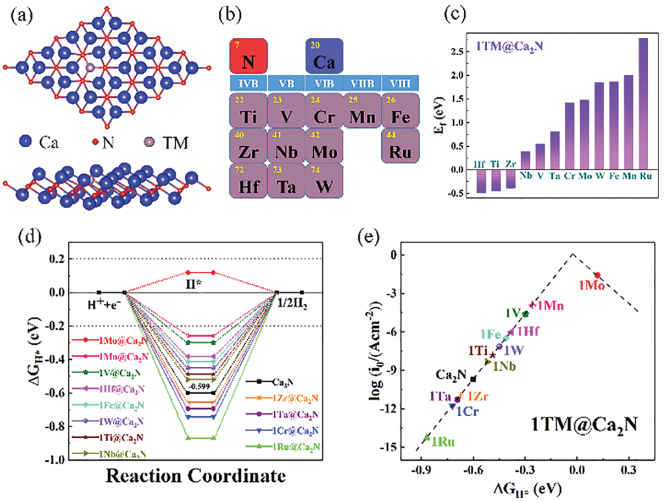

Fig. 2. (a) Top and side view of 1TM@Ca_2N. (b) Brown-red squares refer to the TM dopants. (c) The formation energies for different 1TM@Ca_2N. (d) Calculated Gibbs free energy diagram of HER for 1TM@Ca_2N for a hydrogen coverage of 1/16. The two horizontal black dashed lines correspond to $|\Delta G_{H^*}| < 0.2$ eV. (e) Volcano curves of exchange current density i_0 as a function of ΔG_{H*} for 1TM@Ca_2N.

After determining the stability and conductivity of 1TM@Ca_2N, we studied their HER catalytic activities by calculating the Gibbs free energy ΔG_{H^*}. As shown in Fig. 2d and Table S2 (Supporting information), 8 of 1TM@Ca_2N cases have $|\Delta G_{H^*}|$ smaller than that of Ca_2N monolayer (ΔG_{H^*} = -0.599 eV): 1Mo@Ca_2N (ΔG_{H^*} = 0.119 eV), 1Mn@Ca_2N (ΔG_{H^*} = -0.287 eV), 1V@Ca_2N (ΔG_{H^*} = -0.298 eV), 1Hf@Ca_2N (ΔG_{H^*} = -0.381 eV), 1Fe@Ca_2N (ΔG_{H^*} = -0.442 eV), 1W@Ca_2N (ΔG_{H^*} = -0.449 eV), 1Ti@Ca_2N (ΔG_{H^*} = -0.487 eV) and 1Nb@Ca_2N (ΔG_{H^*} = -0.519 eV). Herein, 1Mo@Ca_2N shows considerable high HER catalytic activity with $|\Delta G_{H^*}| < 0.2$ eV. On the other hand, there are 4 1TM@Ca_2N cases show $|\Delta G_{H^*}|$ larger than Ca_2N monolayer, which are 1Zr@Ca_2N (ΔG_{H^*} = -0.674 eV), 1Ta@Ca_2N (ΔG_{H^*} = -0.692 eV), 1Cr@Ca_2N (ΔG_{H^*} = -0.721 eV) and 1Ru@Ca_2N (ΔG_{H^*} = -0.870 eV). According to the calculated ΔG_{H*} of 12 kinds of 1TM@Ca_2N, it is demonstrated that not all the TM doping can improve the HER catalytic activity of Ca_2N monolayer. The chemical environment has been changed to different degrees, which could result in different catalytic activities. At the same time, we obtained the volcano map according to the relationship between ΔG_{H*} and the exchange current density, as shown in Fig. 2e. The HER catalytic activity of 1Mo@Ca_2N is the best, which is the closest to the top of the volcano map. While the HER catalytic activity of 1Ru@Ca_2N is the worst, it is also furthest away from the top of the volcano map and located at the bottom of the left side of the volcano map.

There are many factors affecting the catalytic activity, such as the replacing position of the doping atoms [55]. To further understand the HER catalytic activity of 1TM@Ca_2N, we selected 4 types of TM (Mo, Mn, V and Hf) atoms to replace the N atom in the $4 \times 4 \times 1$ Ca_2N supercell. However, it is found very difficult to replace the N atom with TM atom, because these cases show very large positive formation energies (Table S3 in Supporting information). It means that the replacing of N atoms are very difficult to achieve with very low thermal stability. Moreover, the HER catalytic activities of these four materials doped with N atom are

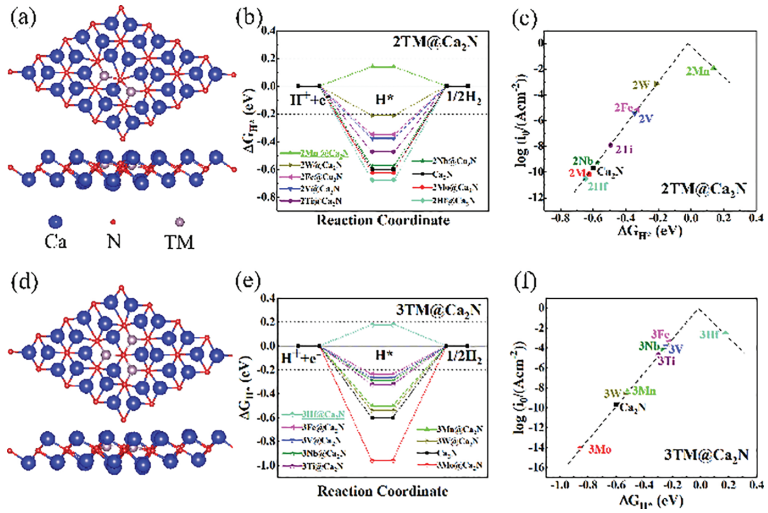

Fig. 3. Top and side views of (a) 2TM@Ca_2N and (d) 3TM@Ca_2N. Calculated Gibbs free energy diagram of HER for (b) 2TM@Ca_2N and (e) 3TM@Ca_2N with the hydrogen coverage of 1/16. The two horizontal black dashed lines correspond to $|\Delta G_{H^*}| < 0.2$ eV. Volcano curves of exchange current density i_0 as a function of ΔG_{H^*} for (c) 2TM@Ca_2N and (f) 3TM@Ca_2N.

not better than those dopants at Ca position. Therefore, it can be known that the strategy of replacing N atoms is not feasible.

Furthermore, $4 \times 4 \times 1$ Ca_2N supercells were doped with different TM content at the position of Ca atom to study the effect of different doping ratios on HER catalytic activity of Ca_2N monolayer. Since not all the 1TM@Ca_2N cases show better HER catalytic activities than Ca_2N monolayer, we selected the HER improved TMs of Ti, Hf, V, Nb, Mo, W, Mn and Fe to study the effect of concentration variation. The structures of replacing 2 and 3 TMs are displayed in Figs. 3a and d, respectively. As listed in Table S1, with the increase of doping ratio, the formation energy is more positive. This is understandable since more doping TM atoms will change the local chemical environment in a stronger way. Among 2TM@Ca_2N and 3TM@Ca_2N, the formation energy of Ti doping is the lowest, which means it is the easiest to be doped into Ca_2N monolayer. On the other hand, W is the most difficult to incorporated with the most positive formation energy. There are signs of charge transfer from TM atoms to the surrounding N atoms for both 2TM@Ca_2N and 3TM@Ca_2N, as shown in Figs. S5b and c (Supporting information), indicating that TM atoms and N atoms are strongly bonded. Although multiple TM doping causes some local changes in the initial structure of Ca_2N monolayer, it does not destroy its metallic conductivity nature (Fig. S6 in Supporting information).

After ensuring the stability and conductivity of 2TM@Ca_2N and 3TM@Ca_2N, we evaluated their HER catalytic activity. As shown in Fig. 3b, we calculated the ΔG_{H*} of 2TM@Ca_2N, and its monolayer. On the other hand, the other 6 kinds of 2TM@Ca_2N have better HER catalytic activity than Ca_2N monolayer, which can be seen that 2Mo@Ca_2N (ΔG_{H*} = -0.626 eV) and 2Hf@Ca_2N (ΔG_{H*} = -0.647 eV) have worse HER catalytic activity than Ca_2N 2Mn@Ca_2N ($\Delta G_{H*} = 0.139$ eV), 2W@Ca_2N (ΔG_{H*} = -0.212 eV), 2Fe@Ca_2N (ΔG_{H*} = -0.329 eV), 2V@Ca_2N (ΔG_{H*} = -0.346 eV), 2Ti@Ca_2N (ΔG_{H*} = -0.493 eV), 2Nb@Ca_2N (ΔG_{H*} = -0.573 eV). Interestingly, the $|\Delta G_{H^*}|$ of 2Mn@Ca_2N is less than 0.2 eV, indicating good HER catalytic activity. In addition, we also calculated the exchange current density (i_0) of these eight materials, and obtained their volcanic diagrams according to the relationship between ΔG_{H^*} and exchange current density (Fig. 3c). The HER catalytic activity of 2Mn@Ca_2N is the best, which is closest to the peak of the volcano plot. While the HER catalytic activity of 2Hf@Ca_2N is the worst, which is the farthest away from the volcano peak.

Furthermore, the catalytic activity of 8 kinds of 3TM@Ca_2N are shown in Fig. 3e. Herein, only 3Mo@Ca_2N (ΔG_{H*} = -0.959 eV) shows worse HER catalytic activity than Ca_2N monolayer. The other 3TM@Ca_2N have better HER catalytic activity than Ca_2N monolayer, which are 3Hf@Ca_2N ($\Delta G_{H*} = 0.178$ eV), 3Fe@Ca_2N ($\Delta G_{H*} = -0.235$ eV), 3V@Ca_2N ($\Delta G_{H*} = -0.268$ eV), 3Nb@Ca_2N ($\Delta G_{H*} = -0.270$ eV), 3Ti@Ca_2N ($\Delta G_{H*} = -0.302$ eV), 3Mn@Ca_2N ($\Delta G_{H*} = -0.522$ eV), 3W@Ca_2N ($\Delta G_{H*} = -0.539$ eV). It is interestingly to find that the $|\Delta G_{H^*}|$ of 3Hf@Ca_2N is smaller than 0.2 eV, indicating the best HER catalytic activity. At the same time, we also calculated the exchange current density of 3TM@Ca_2N according to the previous work (Fig. 3f). Among them, 3Hf@Ca_2N is located on the right side of the volcanic map, which is closest to the peak of the volcanic map. The 3Mo@Ca_2N locates in the lower left corner of the volcano map, which is the farthest away from the vertex of the volcano map. It is noted that, compared with the 2TM@Ca_2N cases, the higher doping ratio of TM do not ensure to achieve better catalytic activity. For example, with the increase of Mo-doping content, the HER catalytic activity is getting worse. But the Fe-doping case shows the opposite trends with the increase of Fe doping content, and its HER catalytic activity is getting better.

In summary, we have systematically studied the potential of two-dimensional electride Ca_2N monolayer as HER catalyst based on density functional theory calculations. We proposed two effective methods to improve the HER catalytic activity of Ca_2N monolayer: vacancy defect engineering and transition metal doping. First of all, the introduction of vacancy defects in Ca_2N monolayer was proposed. Compared with the original Ca_2N monolayer ($\Delta G_{H^*} = -0.599$ eV), Ca_2N-V_{Ca} ($\Delta G_{H^*} = -0.390$ eV) and Ca_2N-V_N ($\Delta G_{H^*} = -0.146$ eV) show improved HER catalytic activities. Secondly, different types and contents transition metals were doped into Ca_2N monolayer. We found that 1Mo@Ca_2N ($\Delta G_{H^*} = 0.119$ eV), 2Mn@Ca_2N ($\Delta G_{H^*} = 0.139$ eV), and 3Hf@Ca_2N ($\Delta G_{H^*} = 0.178$ eV) exhibit excellent HER catalytic activities. This work provides a feasible way to improve the HER properties of 2D electride Ca_2N monolayer for related electrocatalytic applications.

Declaration of competing interest

The authors declare that they have no known competing financial interests or personal relationships that could have appeared to influence the work reported in this paper.

Acknowledgments

This work was supported by the National Natural Science Foundation of China (No. 21973012), the Natural Science Foundation of Fujian Province (Nos. 2020J01474, 2021J06011 and 2020J01351), and the "Qishan Scholar" Scientific Research Project of Fuzhou University.

Supplementary materials

Supplementary material associated with this article can be found, in the online version, at doi:10.1016/j.cclet.2022.06.066.

References

[1] Z.W. Seh, J. Kibsgaard, C.F. Dickens, et al., Science 355 (2017) eaad4998.
[2] Q. Tang, D.E. Jiang, ACS Catal. 6 (2016) 4953–4961.
[3] X. Bai, C. Ling, L. Shi, et al., Sci. Bull. 63 (2018) 1397–1403.
[4] C. Li, D. Zhu, S. Cheng, et al., Chin. Chem. Lett. 33 (2022) 1141–1153.
[5] J. Wang, X. Li, B. Wei, et al., Adv. Funct. Mater. 30 (2020) 1908708.
[6] K. Chen, S. Deng, Y. Lu, et al., Chin. Chem. Lett. 32 (2021) 765–769.
[7] B. Zhang, J. Zhou, Z. Guo, et al., Appl. Surf. Sci. 500 (2020) 144248.
[8] Z. Zheng, L. Yu, M. Gao, et al., Nat. Commun. 11 (2020) 3315.
[9] J. Ban, X. Wen, H. Xu, et al., Adv. Funct. Mater. 31 (2021) 2010472.
[10] Y. Zhou, J. Zhang, E. Song, et al., Nat. Commun. 11 (2020) 2253.
[11] M. Kang, C. Lin, H. Yang, et al., ACS Appl. Mater. Interfaces 13 (2021) 19406–19413.
[12] W. Zhao, B. Jin, L. Wang, et al., Chin. Chem. Lett. 33 (2022) 557–561.
[13] Y. Xu, C. Wang, Y. Huang, J. Fu, Nano Energy 80 (2021) 105545.
[14] Y. Zang, Q. Wu, W. Du, et al., Phys. Rev. Mater. 5 (2021) 045801.
[15] S. Liu, J. Ban, H. Shi, et al., Chem. Eng. J. 431 (2022) 134283.
[16] B. Liu, C. Wu, C. Wen, et al., Electrochim. Acta 408 (2022) 139965.
[17] H. Zeng, S. Chen, Y.Q. Jin, et al., ACS Energy Lett. 5 (2020) 1908–1915.
[18] N. Zheng, X. Li, S. Yan, et al., J. Mater. Chem. 8 (2020) 2376–2386.
[19] C. Wen, Y. Wei, D. Tang, et al., Sci. Rep. 7 (2017) 4907.
[20] A. Liu, X. Liang, X. Ren, et al., Adv. Funct. Mater. 30 (2020) 2003437.
[21] Y. Yu, J. Zhou, Z. Sun, Adv. Funct. Mater. 30 (2020) 2000570.
[22] F. Li, Q. Tang, ACS Appl, Nano Mater. 2 (2019) 7220–7229.
[23] Y.P. Zhu, T.Z. Ren, Z.Y. Yuan, ACS Appl. Mater. Interfaces 7 (2015) 16850–16856.
[24] B. Song, S. Jin, Joule 1 (2017) 220–221.
[25] J. Deng, H. Li, J. Xiao, et al., Energy Environ. Sci. 8 (2015) 1594–1601.
[26] J. Su, L. Zhuang, S. Zhang, et al., Chin. Chem. Lett. 32 (2021) 2947–2962.
[27] S.H. Kang, J. Bang, K. Chung, et al., Sci. Adv. 6 (2020) eaba7416.
[28] L. Liu, C. Wang, L. Zhang, et al., J. Phys. Chem. Lett. 13 (2022) 740–746.
[29] X. Zhang, G. Yang, J. Phys. Chem. Lett. 11 (2020) 3841–3852.
[30] H. Hosono, M. Kitano, Chem. Rev. 121 (2021) 3121–3185.
[31] K. Lee, S.W. Kim, Y. Toda, et al., Nature 494 (2013) 336–340.
[32] J. Li, S. Inagi, T. Fuchigami, et al., Electrochem. Commun. 44 (2014) 45–48.
[33] T. Kocabas, A. Ozden, I. Demiroglu, et al., J. Phys. Chem. Lett. 9 (2018) 4267–4274.
[34] B. Sa, R. Xiong, C. Wen, et al., J. Phys. Chem. C 124 (2020) 7683–7690.
[35] D. Liu, D. Tomanek, Nano Lett. 19 (2019) 1359–1365.
[36] K. Khan, A.K. Tareen, M. Aslam, et al., Prog. Solid State Chem. 54 (2019) 1–19.
[37] M. Kitano, Y. Inoue, Y. Yamazaki, et al., Nat. Chem. 4 (2012) 934–940.
[38] M. Kitano, S. Kanbara, Y. Inoue, et al., Nat. Commun. 6 (2015) 6731.
[39] J.-j. Lin, H.-f. Lv, X.-j. Wu, Chin. J. Chem. Phys. 31 (2018) 649–654.
[40] Y. Lu, J. Li, T. Tada, et al., J. Am. Chem. Soc. 138 (2016) 3970–3973.
[41] J. Wu, J. Li, Y. Gong, et al., Angew. Chem. Int. Ed. 58 (2019) 825–829.
[42] H. Mizoguchi, S.W. Park, K. Kishida, et al., J. Am. Chem. Soc. 141 (2019) 3376–3379.
[43] T.N. Ye, Y. Lu, J. Li, et al., J. Am. Chem. Soc. 139 (2017) 17089–17097.
[44] S. Choi, Y.J. Kim, S.M. Kim, et al., Nat. Commun. 5 (2014) 4881.
[45] S. Zhao, Z. Li, J. Yang, J. Am. Chem. Soc. 136 (2014) 13313–13318.
[46] D.L. Druffel, K.L. Kuntz, A.H. Woomer, et al., J. Am. Chem. Soc. 138 (2016) 16089–16094.
[47] B. Mortazavi, G.R. Berdiyorov, M. Shahrokhi, T. Rabczuk, J. Alloys Compd. 739 (2018) 643–652.
[48] G. Kresse, J. Furthmuller, Phys. Rev. B 54 (1996) 11169–11186.
[49] G.J. Wang, K.Q. Li, L.Y. Peng, et al., Acta Metall. Sin. 58 (2022) 75–88.
[50] G. Wang, L. Peng, K. Li, et al., Comput. Mater. Sci. 186 (2021) 110064.
[51] T. Inoshita, S. Jeong, N. Hamada, H. Hosono, Phys. Rev. X 4 (2014) 031023.
[52] P. Cudazzo, M. Gatti, Phys. Rev. B 96 (2017) 125131.
[53] J.K. Nørskov, T. Bligaard, A. Logadottir, et al., J. Electrochem. Soc. 152 (2005) J23–J26.
[54] J.K. Nørskov, J. Rossmeisl, A. Logadottir, et al., J. Phys. Chem. B 108 (2004) 17886–17892.
[55] C. Ling, Y. Cui, S. Lu, et al., Chem 8 (2022) 1–36.
[56] Z. Huang, W. Luo, L. Ma, et al., Angew. Chem. Int. Ed. 54 (2015) 15181–15185.
[57] Berit Hinnemann, Poul Georg Moses, Jacob Bonde, et al., J. Am. Chem. Soc. 127 (2005) 5308 -5209.
[58] H. Wang, X. Xiao, S. Liu, et al., J. Am. Chem. Soc. 141 (2019) 18578–18584.